Z. Angew. Math. Phys. (2024) 75:211

https://doi.org/10.1007/s00033-024-02347-z

Zeitschrift für angewandte Mathematik und Physik ZAMP

Low-frequency propagating and evanescent waves in strongly inhomogeneous sandwich plates

Ludmila Prikazchikova, Ameya Rege, Julius Kaplunov and Danila Prikazchikov

Abstract. The paper aims at studying dispersion of elastic waves in a sandwich plate with the parameters, characteristic of aerogel core and hard skin layers, typical for aerospace applications including optimal design of fuselage structural components. The proposed approach relies on multiparametric analysis, taking into account the effect of strong transverse inhomogeneity. It is demonstrated that both an additional low-frequency propagating wave and a slowly decaying evanescent one appear due to a high contrast in geometric and mechanical parameters of the layers. The key findings include the derivation of two-mode asymptotic expansions of the full dispersion relation at the low-frequency limit, as well as elucidation of the non-trivial link between long-wave evanescent and propagating modes. A sophisticated composite nature of the obtained expansions involving various shortened forms is investigated. The range of validity for each of these forms over frequency and wave-number domains is evaluated. Comparison of asymptotic results with the numerical solution of the full dispersion relation is presented.

Mathematics Subject Classification. 74A40, 74H10, 74J05, 74K20.

Keywords. Sandwich, Aerogel, Long-wave, Low-frequency, Evanescent, Cut-off, Propagating, Dispersion, High Contrast.

1. Introduction

Sandwich structures have emerged as a remarkable class of materials extensively employed in the modern industry, particularly in aircraft design and construction [1–4]. In the simplest case of a three-layered sandwich plate, they consist of a lightweight core material sandwiched between the two outer layers, typically composed of high-strength materials. The unique design of sandwich plates offers exceptional mechanical properties, including high stiffness and strength-to-weight ratios, making them well-suited for addressing the stringent practical demands, including in particular the implementation for sound insulation in aircrafts.

Sound insulation is essential for creating a quiet and peaceful cabin environment. Aircraft engines, airflow, and aerodynamic forces generate noise, which can cause discomfort and fatigue for passengers and crew. Proper sound insulation materials and techniques help attenuate noise transmission, reducing the overall noise level inside the cabin [5]. At the same time, vibration insulation is another consideration in cabin design [6]. Vibrations caused by engine operation, turbulence, and other sources can create discomfort and adversely affect passenger well-being. Effective insulation materials and structural design techniques help to suppress unwanted vibrations.

With the aim of revolutionising the aircraft (cabin) design, there has been an increasing interest towards developing aerogel-based solutions for aircraft cabin insulation. Aerogels are extremely lightweight materials having ultra-low thermal conductivities and sound velocities [7]. While thermal insulation characteristics have been explored for many decades, a significant amount of research is being carried out recently in understanding their sound insulation characteristics [8], particularly in relation to aircraft applications where they have shown promising potential [9–11]. Aerogels offer several advantages over

Published online: 26 October 2024

traditional insulation materials in aeronautics due to their multifunctional nature, which includes hydrophobicity.

The recent advancements in developing mechanically durable aerogels with property range varying from extremely brittle to highly superflexible have been achieved using the methodologies originating from chemistry and process engineering [12–15]. The stiffness of these materials is very small compared to that of fuselage, e.g. involving aluminium or carbon fibre-reinforced composites. Thus, this practical setup clearly manifests the presence of substantial high contrast in stiffness as well as in density. Moreover, the geometry of aircraft structures of interest also often assumes a considerable contrast in the thickness of stiff and soft layers.

As an example, in this paper we consider a simplified problem for an elastic sandwich in the form of an aerogel-based three-layered plate and present asymptotic results for its dispersive behaviour. The high contrast in thickness, stiffness and density of aluminium skin layers and aerogel core, provides natural small/large parameters, motivating asymptotic treatment. The two characteristic features related to high contrast, including extra low-frequency propagating and evanescent modes are studied. These were earlier observed in [16,17], but the transition of the evanescent waves to the propagating ones have been only recently analysed for the simplest antiplane shear setup [18].

Specific low eigenfrequencies due to high contrast have been first observed in the 1D problem for longitudinal vibrations of a three-component strongly inhomogeneous rod [19], being then extended to multi-component rods [20], multi-span beams [21,22], including random vibrations [23]. Similar manifestation of high contrast emerged in the asymptotic behaviour of the lowest cut-off frequencies for three-layered plates [16,24]. Dispersion analysis of a plane-strain problem in elasticity in [16] revealed the possibility of two-mode long-wave low-frequency approximations. The static limit of the latter contains the previously observed degenerate boundary layers for high-contrast sandwich plates [25–27]. It has become especially clear within the context of antiplane elasticity [17], where in case of antisymmetric motions of a sandwich plate the evanescent mode originating from the relevant static limit may transfer into the shear propagating mode at the lowest cut-off frequency.

The present paper deepens the understanding of the evanescent and propagating modes in application to an aerogel-based sandwich plate with the special focus on the transition from attenuation to propagation. The long-wave low-frequency asymptotic expansions of the full dispersion relation in plane elasticity are derived, taking into consideration the ratios between the contrast parameters including relative thickness, stiffness and density. These ratios support two-mode approximation of the exact dispersion curves, along with a number of shortened approximations over the associated sub-domains of the whole long-wave low-frequency region. The developed framework covers long-wave propagating modes along with two slowly decaying evanescent ones. It is demonstrated that the lowest cut-off frequency belongs to the dispersion curve corresponding to the so-called dynamic edge effect [28], governed by the classical Kirchhoff theory for plate bending. It is also shown that other evanescent mode originates from a slowly decaying static boundary layer earlier observed in [25,26] for the antiplane shear.

The paper is organised as follows. The problem is formulated in Sect. 2. The asymptotic analysis for both propagating and evanescent modes is performed in Sect. 3. Numerical illustrations, including comparison of exact and approximate results, are presented in Sect. 4.

2. Governing equations

Consider a three-layered symmetric elastic plate, composed of isotropic layers, with the core layer of thickness $2h_c$ and the skin layers of thickness h_s, see Fig. 1. Here and below the index 'c' and 's' is associated with the core and skin layers, respectively. Remark that a number of realistic scenarios involving aerogels, e.g. see [9–11], may also include extra acoustic layers between core and skin ones. However, for the sake of simplicity, their presence is not taken into consideration in what follows.

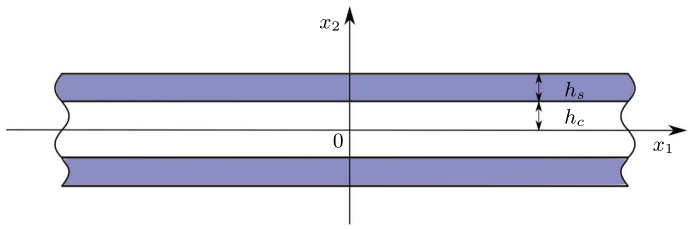

FIG. 1. A three-layered plate

The governing equations of plane-strain motion are taken in the conventional form

$$\sigma^q_{ij,j} = \rho_q u^q_{i,tt}, \quad i = 1, 2, \quad q = c, s, \tag{1}$$

where σ^q_{ij} are stresses, u^q_i are displacements, ρ_q are volume mass densities. Note that a comma in the suffix indicates differentiation with respect to appropriate spacial or time variable; summation over the repeated suffixes is also assumed. The constitutive relations of linear isotropic elasticity are written as

$$\sigma^q_{ij} = \lambda_q u^q_{k,k}\delta_{ij} + \mu_q(u^q_{i,j} + u^q_{j,i}), \tag{2}$$

where λ_q and μ_q are the Lamé parameters. The traction-free boundary conditions along the faces $x_2 = \pm(h_c + h_s)$ are imposed, together with continuity conditions along the interfaces $x_2 = \pm h_c$. They are given by

$$\sigma^s_{i2} = 0 \qquad \text{at} \quad x_2 = \pm(h_c + h_s) \tag{3}$$

and

$$\sigma^c_{i2} = \sigma^s_{i2}, \quad u^c_i = u^s_i, \qquad \text{at} \quad x_2 = \pm h_c, \tag{4}$$

where $i = 1, 2$.

The dispersion relation for the antisymmetric modes of the three-layered plate takes a rather sophisticated form, e.g. see [29] and [16]. It is

$$\begin{aligned}
&4K^2h^3\alpha_s\beta_s F_4\left[F_1F_2C_{\beta_c}S_{\alpha_c} - 2\alpha_c\beta_c(\varepsilon-1)F_3C_{\alpha_c}S_{\beta_c}\right]\\
&\quad + h\alpha_s\beta_s C_{\alpha_s}C_{\beta_s}\left[4\alpha_c\beta_c K^2\left(h^4F_3^2 + {F_4}^2(\varepsilon-1)^2\right)C_{\alpha_c}S_{\beta_c}\right.\\
&\quad \left. - \left(4K^4h^4F_2^2 + {F_4}^2F_1^2\right)S_{\alpha_c}C_{\beta_c}\right]\\
&\quad + C_{\beta_s}S_{\alpha_s}\varepsilon\beta_s(\beta_s^2 - K^2h^2)(\beta_c^2 - K^2)\left[4\alpha_s^2\beta_c K^2h^2S_{\alpha_c}S_{\beta_c} - {F_4}^2\alpha_c C_{\alpha_c}C_{\beta_c}\right]\\
&\quad + C_{\alpha_s}S_{\beta_s}\varepsilon\alpha_s(\beta_s^2 - K^2h^2)(\beta_c^2 - K^2)\left[4\alpha_c\beta_s^2K^2h^2C_{\alpha_c}C_{\beta_c} - {F_4}^2\beta_c S_{\alpha_c}S_{\beta_c}\right]\\
&\quad + h^3S_{\alpha_s}S_{\beta_s}\left[\left(4\alpha_s^2\beta_s^2K^2F_1^2 + K^2{F_4}^2F_2^2\right)C_{\beta_c}S_{\alpha_c}\right.\\
&\quad \left. - \alpha_c\beta_c\left(16\alpha_s^2\beta_s^2(\varepsilon-1)^2K^4 + {F_4}^2F_3^2\right)C_{\alpha_c}S_{\beta_c}\right] = 0,
\end{aligned} \tag{5}$$

where

$$\begin{aligned}
F_1 &= 2(\varepsilon-1)K^2 - \varepsilon\Omega^2,\\
F_2 &= 2(\varepsilon-1)K^2 + \frac{\varepsilon(1-r)}{r}\,\Omega^2,\\
F_3 &= 2(\varepsilon-1)K^2 + \frac{\varepsilon}{r}\,\Omega^2,\\
F_4 &= \beta_s^2 + K^2h^2,
\end{aligned} \tag{6}$$

Table 1. *Material parameters*

Material	Density kg/m^3	Young's modulus Pa	Poisson's ratio
Aluminium	2750	7.17×10^{10}	0.331
Aerogel	100	2.26×10^{5}	0.200

and

$$\alpha_c^2 = K^2 - \varkappa_c^2\Omega^2, \quad \alpha_s^2 = h^2\left(K^2 - \frac{\varepsilon\varkappa_s^2}{r}\,\Omega^2\right),$$
$$\beta_c^2 = K^2 - \Omega^2, \quad \beta_s^2 = h^2\left(K^2 - \frac{\varepsilon}{r}\,\Omega^2\right). \tag{7}$$

In the above $C_{\alpha_q} = \cosh(\alpha_q)$, $C_{\beta_q} = \cosh(\beta_q)$, $S_{\alpha_q} = \sinh(\alpha_q)$, $S_{\beta_q} = \sinh(\beta_q)$, and $\varkappa_q = c_{2q}/c_{1q}$ with

$$c_{1q}^2 = \frac{\lambda_q + 2\mu_q}{\rho_q}, \quad c_{2q}^2 = \frac{\mu_q}{\rho_q}, \quad q = c, s. \tag{8}$$

The dimensionless frequency Ω and wave number K are introduced as

$$\Omega = \frac{\omega h_c}{c_{2c}}, \qquad K = kh_c, \tag{9}$$

together with the dimensionless problem parameters

$$h = \frac{h_s}{h_c}, \qquad \varepsilon = \frac{\mu_c}{\mu_s}, \qquad r = \frac{\rho_c}{\rho_s}, \tag{10}$$

expressing the contrast in thickness, stiffness and density of the layers.

In this paper, we analyse an aerogel-based sandwich plate with the material parameters of the layers given in Table 1, where the characteristics of a super-flexible hybrid silica aerogel are presented. The thickness of the core layer is $2h_c = 0.020\,\mathrm{m}$, while the outer layers are of the thickness $h_s = 0.002\,\mathrm{m}$.

3. Asymptotic analysis

3.1. Parametric setup

On setting $K = 0$ in dispersion relation (5), we obtain the equation for cut-off frequencies, given by

$$\tan(\Omega)\tan\left(\sqrt{\frac{\varepsilon}{r}}\,h\,\Omega\right) = \sqrt{\varepsilon\, r}, \tag{11}$$

see also a similar equation for the eigenfrequencies of a three-component elastic rod in [19]. It follows readily from (11) that for the contrast parameters satisfying

$$r \ll h \ll \varepsilon^{-1}, \tag{12}$$

the so-called global low-frequency regime occurs, see [16,20]. This regime supports a polynomial variation displacements across the thickness of the plate. In this case, we have for the lowest cut-off frequency at leading order

$$\Omega_{sh} \approx \sqrt{\frac{r}{h}} \ll 1. \tag{13}$$

This frequency corresponds to shear motion of the plate, see [16,24].

TABLE 2. *Asymptotic behaviour of the coefficients in expansion* (15)

Terms	Order of γ_i	Coefficients G_i
$\gamma_1\Omega^2$	$\gamma_1 \sim h^{11}$	$G_1 = -\dfrac{\varepsilon_0^4}{r_0^3}$
$\gamma_2 K^4$	$\gamma_2 \sim h^5$	$G_2 = -\dfrac{4\varepsilon_0^3(\varkappa_2^2-1)}{r_0^2}$
$\gamma_3 K^2\Omega^2$	$\gamma_3 \sim h^4$	$G_3 = \dfrac{4\varepsilon_0^3(\varkappa_2^2-1)}{r_0^3}$
$\gamma_4 K^6$	$\gamma_4 \sim 1$	$G_4 = \dfrac{4\varepsilon_0^2(\varkappa_2^2-1)^2}{3r_0^2}$
$\gamma_5\Omega^4$	$\gamma_5 \sim h^{10}$	$G_5 = \dfrac{\varepsilon_0^4}{r_0^4}$
$\gamma_6 K^4\Omega^2$	$\gamma_6 \sim h^4$	$G_6 = \dfrac{4\varepsilon_0^3(\varkappa_1^2+1)(\varkappa_2^2-1)}{3r_0^3}$
$\gamma_7 K^8$	$\gamma_7 \sim 1$	$G_7 = \dfrac{4\varepsilon_0^2(\varkappa_1^2+1)(\varkappa_2^2-1)^2}{9r_0^2}$
$\gamma_8 K^2\Omega^4$	$\gamma_8 \sim h^4$	$G_8 = -\dfrac{2\varepsilon_0^3(3\varkappa_1^2+1)(\varkappa_2^2-1)}{3r_0^3}$
$\gamma_9 K^6\Omega^2$	$\gamma_9 \sim 1$	$G_9 = -\dfrac{2\varepsilon_0^2(3\varkappa_1^2+1)(\varkappa_2^2-1)^2}{9r_0^2}$
$\gamma_{10} K^{10}$	$\gamma_{10} \sim 1$	$G_{10} = \dfrac{4\varepsilon_0^2(\varkappa_1^2+1)(\varkappa_2^2-1)^2}{45r_0^2}$

The studied setup for the aerogel-based sandwich plate, see Table 1, motivates the scaling

$$h \ll 1, \quad r \sim h^2, \qquad \varepsilon \sim h^8, \tag{14}$$

which is in agreement with conditions (12), implying that $\Omega_{sh} \sim \sqrt{h}$ in formula (13). Note that scaling (14) is not unique and there is a room for the choice of the powers of the main small parameter. This sort of uncertainty is hardly avoidable in applied research. For comparison, an alternative parametric setup is discussed in the Appendix.

Now, the dispersion relation (5) can be expanded in Taylor series over the long-wave low-frequency region ($K \ll 1$, $\Omega \ll 1$), resulting in the polynomial equation

$$\begin{aligned}\gamma_1\Omega^2 + \gamma_2 K^4 + \gamma_3 K^2\Omega^2 + \gamma_4 K^6 + \gamma_5\Omega^4 + \gamma_6 K^4\Omega^2 + \gamma_7 K^8 \\ + \gamma_8 K^2\Omega^4 + \gamma_9 K^6\Omega^2 + \gamma_{10} K^{10} + \ldots = 0,\end{aligned} \tag{15}$$

where the coefficients γ_i, $i = 1, \ldots 10$, can be found in Appendix A in [16]. Using relations $r = r_0 h^2$ and $\varepsilon = \varepsilon_0 h^8$ ($r_0 \sim 1$, $\varepsilon_0 \sim 1$), based on scaling (14), the leading order estimations for γ_i can be presented in the form $\gamma_i \approx G_i h^{a_i}$ ($G_i \sim 1$) and a_i are constants. These are summarised in the following Table 2.

3.2. Fundamental mode

Analysis of the fundamental mode can be started with the classical Kirchhoff theory for plate bending, dictating that $\gamma_1\Omega^2 \sim \gamma_2 K^4$, e.g. see [30]. This results in relation $\Omega^2 \sim h^{-6}K^4$, underlying the following

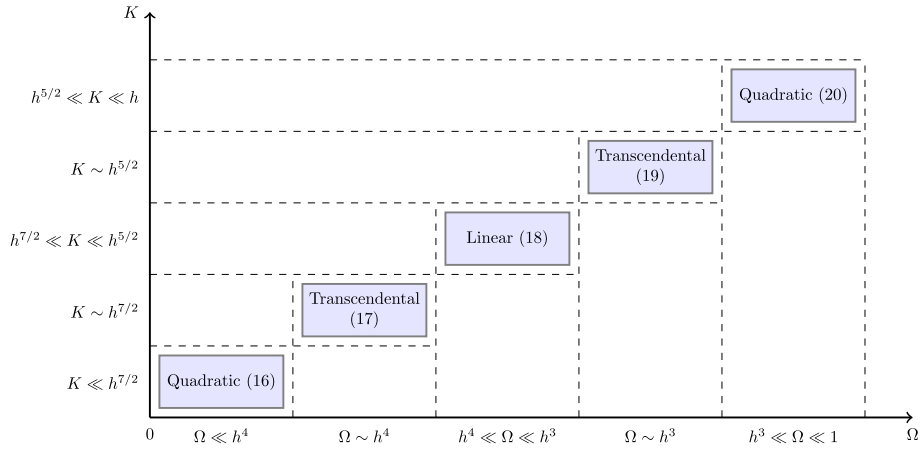

FIG. 2. Sub-domains for shortened approximations (16)–(20) of the fundamental mode

estimates in (15)

$$\gamma_1\Omega^2 \sim h^5K^4, \qquad \gamma_6K^4\Omega^2 \sim h^{-2}K^8,$$
$$\gamma_2K^4 \sim h^5K^4, \qquad \gamma_7K^8 \sim K^8,$$
$$\gamma_3K^2\Omega^2 \sim h^{-2}K^6, \qquad \gamma_8K^2\Omega^4 \sim h^{-8}K^{10},$$
$$\gamma_4K^6 \sim K^6, \qquad \gamma_9K^6\Omega^2 \sim h^{-6}K^{10},$$
$$\gamma_5\Omega^4 \sim h^{-2}K^8, \qquad \gamma_{10}K^{10} \sim K^{10}.$$

Hence, we have

$$h^6G_1\Omega^2 + G_2K^4 = 0, \qquad \text{at} \qquad \Omega \ll h^4, \quad K \ll h^{7/2}. \tag{16}$$

Next, at $\Omega \sim h^4$ and $K \sim h^{7/2}$, we arrive at

$$h^7G_1\Omega^2 + hG_2K^4 + G_3K^2\Omega^2 = 0. \tag{17}$$

Now, consider the sub-domain $\Omega \gg h^4$ and $K \gg h^{7/2}$. It can be easily verified that the leading order terms are γ_2K^4 and $\gamma_3K^2\Omega^2$. Therefore, $\Omega^2 \sim hK^2$, leading to

$$hG_2K^2 + G_3\Omega^2 = 0, \qquad \text{at} \qquad h^4 \ll \Omega \ll h^3, \quad h^{7/2} \ll K \ll h^{5/2}. \tag{18}$$

At $\Omega \sim h^3$ and $K \sim h^{5/2}$, we obtain three leading order terms γ_2K^4, $\gamma_3K^2\Omega^2$ and γ_4K^6, implying

$$h^5G_2K^2 + h^4G_3\Omega^2 + G_4K^4 = 0. \tag{19}$$

Proceeding further, we have

$$h^4G_3\Omega^2 + G_4K^4 = 0, \qquad \text{at} \qquad h^3 \ll \Omega \ll 1, \quad h^{5/2} \ll K \ll h. \tag{20}$$

Finally, the uniform asymptotic expansion for the fundamental mode becomes

$$h^{11}G_1\Omega^2 + h^5G_2K^4 + h^4G_3K^2\Omega^2 + G_4K^6 = 0, \tag{21}$$

over the domain $\Omega \ll 1$ and $K \ll h$.

The sub-domains corresponding to shortened relations (16)–(20) are displayed in Fig. 2. It is worth noting that the dispersive behaviour includes quadratic, see (16) and (20), linear (18) and transcendental, see (17) and (19), approximations.

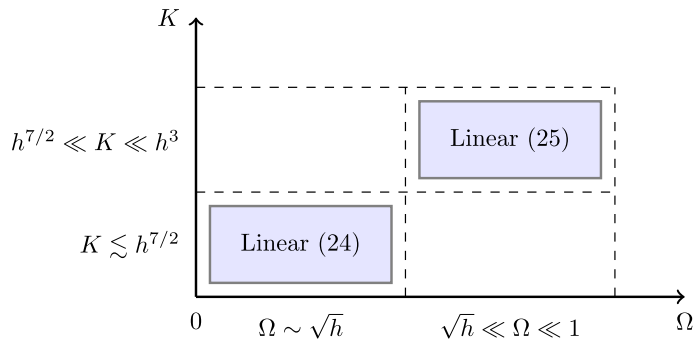

FIG. 3. Sub-domains for shortened approximations (24)–(25) for the first shear mode

3.3. First shear harmonic

First, on setting $K = 0$ in expansion (15), we derive an approximate polynomial equation for the cut-off frequency. It takes form

$$hG_1\Omega^2 + G_5\Omega^4 = \Omega^2(\Omega^2 - \Omega_{sh}^2) = 0, \tag{22}$$

where $\Omega_{sh}^2 = -hG_1/G_5 = r_0 h \sim h$. Now we can estimate the terms in (15) over the vicinity of the cut-off frequency, where $\Omega \sim \sqrt{h}$. Then, we have

$$\begin{aligned}
&\gamma_1\Omega^2 \sim h^{12}, && \gamma_6 K^4\Omega^2 \sim h^5 K^4,\\
&\gamma_2 K^4 \sim h^5 K^4, && \gamma_7 K^8 \sim K^8,\\
&\gamma_3 K^2\Omega^2 \sim h^5 K^2, && \gamma_8 K^2\Omega^4 \sim h^6 K^2,\\
&\gamma_4 K^6 \sim K^6, && \gamma_9 K^6\Omega^2 \sim hK^6,\\
&\gamma_5\Omega^4 \sim h^{12}, && \gamma_{10} K^{10} \sim K^{10}.
\end{aligned} \tag{23}$$

Assuming in (23) that the term $\gamma_3 K^2\Omega^2$ is much greater than $\gamma_4 K^6$, we deduce

$$h^7 G_1 + G_3 K^2 + h^6 G_5\Omega^2 = 0, \qquad \text{at} \quad K \lesssim h^{7/2}. \tag{24}$$

Another near cut-off approximation takes the form

$$G_3 K^2 + h^6 G_5\Omega^2 = 0, \qquad \text{at} \quad h^{7/2} \ll K \ll h^3. \tag{25}$$

Obviously, the uniform approximation for this mode is given by (24). The diagram, demonstrating the areas of validity for asymptotic behaviours (24)–(25), is presented in Fig. 3.

3.4. Two-mode approximation for propagating modes

Long-wave low-frequency approximations for fundamental mode (21) and first harmonic (24) can be combined. As a result, we arrive at the two-mode approximation

$$h^{10} G_5\Omega^4 + h^4(h^7 G_1 + G_3 K^2)\Omega^2 + K^4(h^5 G_2 + G_4 K^2) = 0, \tag{26}$$

valid at $K \ll h$ and $\Omega \ll 1$.

3.5. Slowly decaying evanescent modes

Taking first the static limit, $\Omega = 0$, in expansion (15) and neglecting $O(K^8)$ terms, we obtain

$$K^4(h^5 G_2 + G_4 K^2) = 0. \tag{27}$$

The fourth-order root, $K = 0$, always appears in the classical theory for plate bending, while the small root

$$K = i\sqrt{\frac{3\varepsilon_0}{1-\varkappa_s^2}}h^{5/2}, \tag{28}$$

is typical of the considered high-contrast setup. It determines the decay rate which is much greater than the sandwich thickness. Earlier, similar roots were observed for antiplane shear of a three-layered high-contrast plate, see [25,26].

Next, consider the effect of small frequency ($\Omega < \Omega_{sh}$) on the evanescent waves. As might be expected, the perturbation of the zero root, $K = 0$, can be found from the dispersion relation similar to that in the classical plate theory. In this case, we have the same approximation, see (16), as for the related propagating mode, which is valid at $|K| \ll h^{7/2}$ and $\Omega \ll h^4$. This mode is often referred to as the dynamic edge effect, e.g. see [28]. At $|K| \sim h^{7/2}$ and $\Omega \sim h^4$ we also have the same estimate as for the propagating mode, see (17). Only at $\Omega \gg h^4$, the estimate for this evanescent wave differs from that for the fundamental propagating mode, given by (18). In this case

$$h^7 G_1 + G_3 K^2 = 0, \tag{29}$$

valid at $h^4 \ll \Omega \ll \sqrt{h}$ and $|K| \sim h^{7/2}$.

Over a vicinity of the cut-off frequency, where $\Omega \sim \sqrt{h}$ and $|K| \sim h^{7/2}$, we now arrive at formula (24) corresponding to the shear propagating mode. The uniform behaviour of the evanescent mode is

$$h^7 G_1 \Omega^2 + h G_2 K^4 + G_3 K^2 \Omega^2 + h^6 G_5 \Omega^4 = 0. \tag{30}$$

It is valid over the domain $\Omega \lesssim \sqrt{h}$ and $|K| \lesssim h^{7/2}$.

Next, consider a low-frequency perturbation of the small imaginary root K, see (28). At $\Omega \ll h^3$, it manifests a quasi-static behaviour, governed by

$$h^5 G_2 + G_4 K^2 = 0. \tag{31}$$

Then, at $|K| \sim h^{5/2}$ and $\Omega \sim h^3$, we have

$$h^5 G_2 K^2 + h^4 G_3 \Omega^2 + G_4 K^4 = 0. \tag{32}$$

Finally, at $h^{5/2} \ll |K| \ll h$ and $h^3 \ll \Omega \ll 1$, we derive

$$h^4 G_3 \Omega^2 + G_4 K^4 = 0. \tag{33}$$

The associated uniform asymptotic relation is given by

$$h^5 G_2 K^2 + h^4 G_3 \Omega^2 + G_4 K^4 = 0, \tag{34}$$

valid at $|K| \ll h$ and $\Omega \ll 1$.

It is remarkable that the two-mode approximation for the slowly decaying evanescent modes takes the same form (26) as that for the propagating modes. A summary of the asymptotic regimes for the considered evanescent modes is displayed below in Figs. 4 and 5.

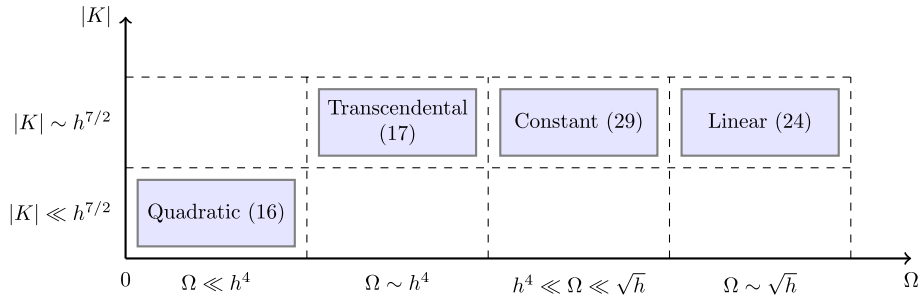

FIG. 4. Asymptotic behaviour of the evanescent mode related to the dynamic edge effect

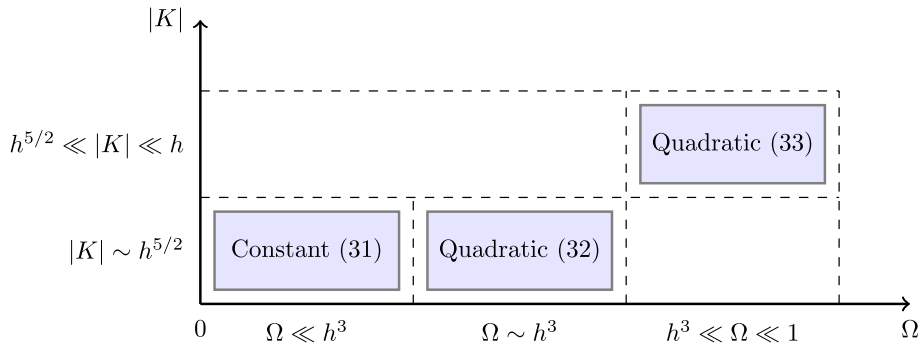

FIG. 5. Asymptotic behaviour of the extra evanescent mode due to high contrast

4. Numerical results

The graphical illustrations below contain comparisons of dispersion curves, corresponding to the full dispersion relation with approximate ones relying on the derived asymptotic expansions. In the figures below the exact data are shown by solid lines, whereas the asymptotic results are depicted by dashed lines, with the problem parameters listed in Table 1. Figures 6, 7 and 8 correspond to propagating modes. In Fig. 6a the fundamental mode calculated from full dispersion relation (5) is presented, along with its uniform approximation (21). Figure 6b shows the first shear mode, corresponding to dispersion relation (5) and its approximation (24). Figure 8 demonstrates both fundamental and shear modes together with two-mode approximation (26). These figures reveal that the chosen high-contrast parameters support remarkably long shear waves.

Figures 8 and 9 correspond to evanescent waves. Figure 8a illustrates the dynamic edge effect [28], with the associated dispersion curve first growing from the origin and then decaying towards the cut-off frequency. Figure 8b demonstrates the extra evanescent wave in a finer scale, see (28) and also [26]. Finally, Fig. 9 shows two-mode approximation (26) for both evanescent waves.

The presented numerical results also indicate that the extra low-frequency shear wave originates from the classical evanescent wave, corresponding to the dynamic edge effect, in contrast to the antiplane problem for the same sandwich plate, see [18]. In the latter case, in the absence of dynamic edge effect, the extra propagating and evanescent waves are related to each other.

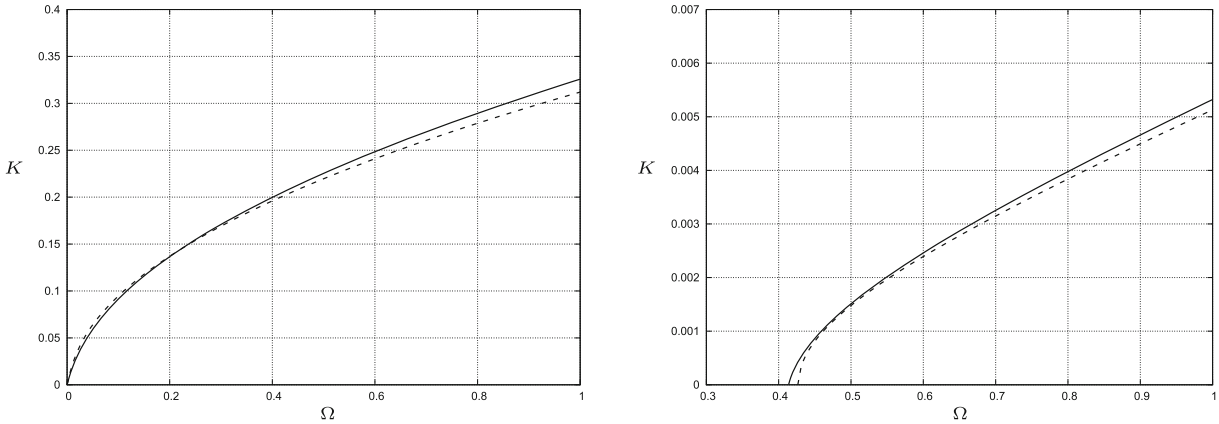

(A) Fundamental mode (B) Shear mode

FIG. 6. Exact dispersion relation (5) (solid line) in (**a**) and (**b**), uniform asymptotic expansion (21) for the fundamental mode (dashed line in (**a**)) and uniform asymptotic expansion (24) for the shear mode (dashed line in (**b**))

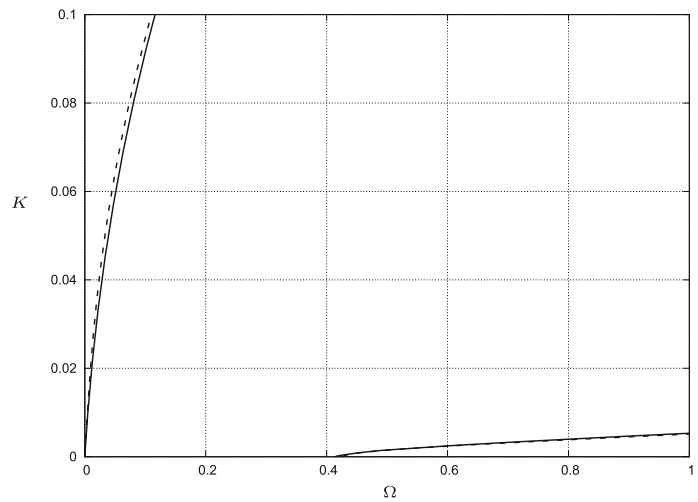

FIG. 7. Exact dispersion relation (5) (solid line) and two-mode asymptotic expansion (26) (dashed line)

5. Conclusion

Dispersion of plane elastic waves in an aerogel-based sandwich plate has been analysed. It has been shown that both extra low-frequency propagating mode and a slowly decaying evanescent one emerge as a result of high contrast in problem parameters. Two-mode long-wave low-frequency asymptotic approximation of the full dispersion relation is derived, appearing to be valid for both propagating and evanescent waves.

It has been demonstrated that the transition from the evanescent modes to the extra propagating one is different to that for the scalar antiplane case as illustrated in [18]. In the latter case, in the absence of the dynamic edge effect, extra propagating and evanescent modes are related to each other, while the analysis in this paper shows that the extra propagating mode originates from the aforementioned dynamic edge effect.

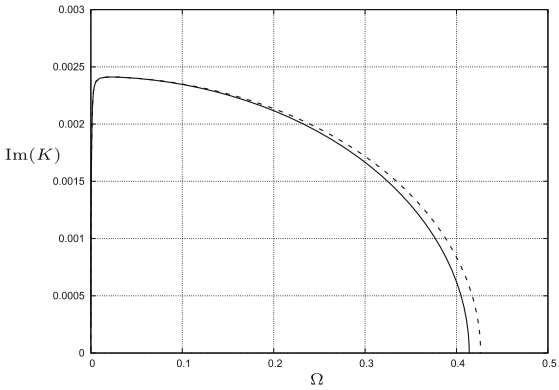

(A) Evanescent mode related to the dynamic edge effect

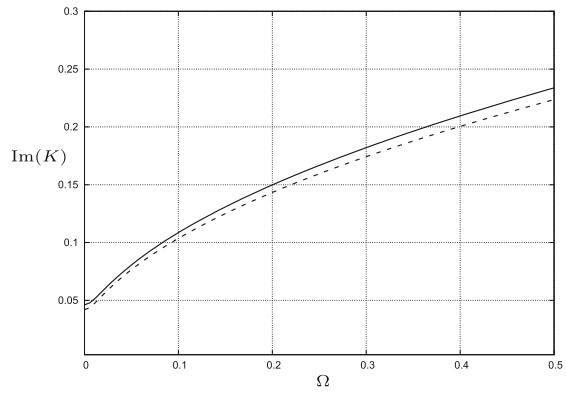

(B) Extra evanescent mode due to high contrast

FIG. 8. Exact dispersion relation (5) (solid line) in **a** and **b** and uniform asymptotic expansion (30) (dashed line in (**a**)) for the evanescent mode originated from the dynamic edge effect and uniform asymptotic expansion (34) (dashed line in (**b**)) for the extra evanescent mode due to high contrast

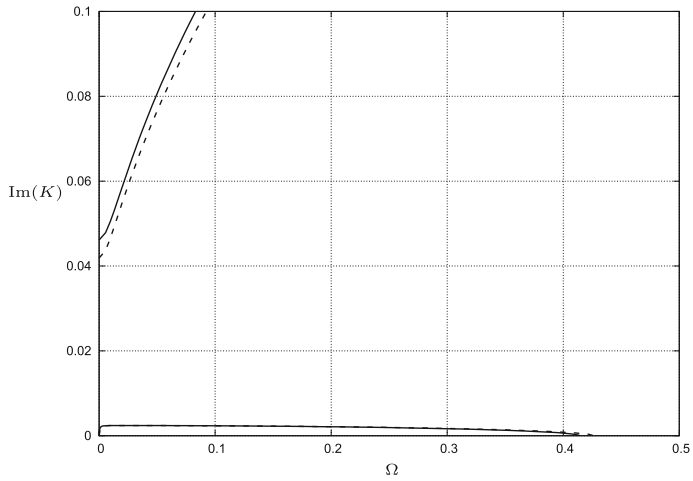

FIG. 9. Exact dispersion relation (5) (solid line) and two-mode expansion (26) (dashed line) for evanescent modes

A variety of shortened approximate relations have been also formulated for each mode. The diagrams in Figs. 2, 3, 4 and 5 manifest domains of validity of the aforementioned relations, highlighting their highly nontrivial composite nature. The full dispersion relation is taken as a natural benchmark for all the numerical comparisons.

The paper is restricted to the assumption that the aerogel behaviour is governed by linear isotropic elasticity. This assumption could be justified within the considered frequency range for a diverse range of aerogels. At the same time, the current setup could be refined, by accounting for microstructure and dissipative properties. Also, a sandwich of finite length can be potentially considered, using appropriate boundary conditions arising as a generalisation of the Saint-Venant's principle, see [17,31]. The developed procedure may also be extended to functionally graded structures, e.g. see [32], prospective for modelling a number of aerogel-based composites.

The consideration in the paper broadens the existing knowledge on the dispersive behaviour of complex systems, characterised by several parameters. Previous efforts in this area were focussed not only on high-contrast laminates [16,18], but also on homogeneous shells and beams, see [33,34].

Acknowledgements

LP and AR gratefully acknowledge the support of the Engineering and Physical Sciences Research Council, UK [EP/Y021983/1].

Author contributions JK and AR contributed on conceptualisation and methodology. DP and LP performed formal analysis and prepared an original draft. LP carried out visualisation of the obtained results. All authors reviewed the manuscript.

Data Availability No datasets were generated or analysed during the current study.

Declarations
Conflict of interest The authors declare no Conflict of interest.

Appendix

In Sect. 3 we take the scaling of the problem parameters in form (14). In fact, a unique scaling is hardly possible for real-world applications. In particular, for the scenario in Sect. 3, we could potentially start from the relations

$$h \ll 1, \qquad r \sim h^2, \qquad \varepsilon \sim h^{31/4}, \tag{35}$$

which differ from those in (14) in the estimate for parameter ε only. In this case, the first cut-off shear frequency is again $\Omega_{sh} \sim \sqrt{h}$. Following similar procedure as in Sect. 3, we arrive at the uniform asymptotic expansion for the fundamental mode given by

$$h^{21/2} G_1 \Omega^2 + h^{19/4} G_2 K^4 + h^{15/4} G_3 K^2 \Omega^2 + G_4 K^6 = 0, \tag{36}$$

valid at $K \ll h^{15/16}$ and $\Omega \ll 1$. For the first shear cut-off mode the uniform asymptotic expansion becomes

$$h^{21/2} G_1 + h^{15/4} G_3 K^2 + h^{19/2} G_5 \Omega^2 = 0, \tag{37}$$

where $K \ll h^{23/8}$ and $\Omega \ll 1$. Finally, a two-mode approximation may be constructed from the above two, giving

$$h^{21/2} G_1 \Omega^2 + h^{19/4} G_2 K^4 + h^{15/4} G_3 K^2 \Omega^2 + G_4 K^6 + h^{19/2} G_5 \Omega^4 = 0, \tag{38}$$

$K \ll h^{15/16}$, $\Omega \ll 1$.

In spite of the difference between formulae (14) and (35), resulting in not entirely identical coefficients in the related approximations of the full dispersion relation, the dispersion curves presented in Sect. 4 are also quite suitable for illustrating the asymptotic expansions in the Appendix.

References

[1] Vinson, J.R.: Sandwich structures. Appl. Mech. Rev. **54**(3), 201–214 (2001)
[2] Clarkson, B.L., Mead, D.J.: High frequency vibration of aircraft structures. J. Sound Vib. **28**(3), 487–504 (1973)
[3] Sturm, R., Klett, Y., Kindervater, Ch., Voggenreiter, H.: Failure of CFRP airframe sandwich panels under crash-relevant loading conditions. Compos. Struct. **112**, 11–21 (2014)
[4] Castanié, B., Bouvet, C., Ginot, M.: Review of composite sandwich structure in aeronautic applications. Compos. C: Open Access **1**, 100004 (2020)
[5] Heitman, K.E., Mixson, J.S.: Laboratory study of cabin acoustic treatments installed in an aircraft fuselage. J. Aircr. **23**(1), 32–38 (1986)
[6] Li, Z., Crocker, M.J.: A review on vibration damping in sandwich composite structures. Int. J. Acoust. Vib. **10**(4), 159–169 (2005)
[7] Hüsing, N., Schubert, U.: Aerogels-airy materials: chemistry, structure, and properties. Angew. Chem. Int. Edit. **37**(1–2), 22–45 (1998)
[8] Budtova, T., Lokki, T., Malakooti, S., Rege, A., Lu, H., Milow, B., Vapaavuori, J., Vivod, S.L.: Acoustic properties of aerogels: current status and prospects. Adv. Eng. Mater. **25**(6), 2201137 (2023)
[9] Zverev, A.Y.: Noise control mechanisms of inside aircraft. Acoust. Phys. **62**, 478–482 (2016)
[10] Hesse, C., Allebrodt, P., Rege, A.: Multi-Physikalische Untersuchungen zum Transmissionsverhalten neuartiger Kabinenseitenwände. Deutsche Gesellschaft für Luft-und Raumfahrt-Lilienthal-Oberth eV, Bonn (2020)
[11] Gillner, CH., Marckmann, H., Dilba, B., Zaleski, O., Vöpel, P., Dzierbinski, A., Okumus, E., Milow, B.: Aerogels as innovative insulation materials - a range of acoustic properties. Fortschritte der Akustik-DAGA 2021-47. Jahrestagung für Akustik (2021)
[12] Wong, J.C., Kaymak, H., Brunner, S., Koebel, M.M.: Mechanical properties of monolithic silica aerogels made from polyethoxydisiloxanes. Microporous Mesoporous Mater. **183**, 23–29 (2014)
[13] Schwan, M., Naikade, M., Raabe, D., Ratke, L.: From hard to rubber-like: mechanical properties of resorcinol-formaldehyde aerogels. J. Mater. Sci. **50**, 5482–5493 (2015)
[14] Rege, A., Voepel, P., Okumus, E., Hillgärtner, M., Itskov, M., Milow, B.: Temperature-dependent stiffening and inelastic behavior of newly synthesized fiber-reinforced super flexible silica aerogels. Mater **12**(18), 2878 (2019)
[15] Rege, A., Schwan, M., Chernova, L., Hillgärtner, M., Itskov, M., Milow, B.: Microstructural and mechanical characterization of carbon aerogels: an in-situ and digital image correlation-based study. J. Non-Cryst. Solids **529**, 119568 (2020)
[16] Kaplunov, J., Prikazchikov, D.A., Prikazchikova, L.A.: Dispersion of elastic waves in a strongly inhomogeneous three-layered plate. Int. J. Solids Struct. **113**, 169–179 (2017)
[17] Kaplunov, J., Prikazchikova, L., Alkinidri, M.: Antiplane shear of an asymmetric sandwich plate. Continuum Mech. Therm. **33**(4), 1247–1262 (2021)
[18] Aghalovyan, L.A., Ghulghazaryan, L.G., Kaplunov, J., Prikazchikov, D.: Degenerated boundary layers and long-wave low-frequency motion in high-contrast elastic laminates. Mathematics **11**(18), 3905 (2023)
[19] Kaplunov, J., Prikazchikov, D., Sergushova, O.: Multi-parametric analysis of the lowest natural frequencies of strongly inhomogeneous elastic rods. J. Sound Vib. **366**, 264–276 (2016)
[20] Kaplunov, J., Prikazchikov, D.A., Prikazchikova, L.A., Sergushova, O.: The lowest vibration spectra of multi-component structures with contrast material properties. J. Sound Vib. **445**, 132–147 (2019)
[21] Şahin, O., Erbaş, B., Kaplunov, J., Savšek, T.: The lowest vibration modes of an elastic beam composed of alternating stiff and soft components. Arch. Appl. Mech. **90**, 339–352 (2020)
[22] Şahin, O.: On the lowest frequencies of strongly inhomogeneous multicomponent beams. Math. Method. Appl. Sci. **44**(11), 9302–9314 (2021)
[23] Elishakoff, I., Fang, T., Jiang, C.: Free, forced, and random vibrations of a beam composed of highly contrasting materials. Appl. Math. Model. **89**, 1696–1720 (2021)
[24] Prikazchikova, L., Ece Aydın, Y., Erbaş, B., Kaplunov, J.: Asymptotic analysis of an anti-plane dynamic problem for a three-layered strongly inhomogeneous laminate. Math. Mech. Solids **25**(1), 3–16 (2020)
[25] Baxter, S.C., Horgan, C.O.: End effects for anti-plane shear deformations of sandwich structures. J. Elast. **40**, 123–164 (1995)
[26] Horgan, C.O.: Saint-Venant end effects for sandwich structures. Fourth Int. Conf. Sanwich Construct. **1**, 191–200 (1998)

[27] Avila-Pozos, O., Movchan, A.B.: Slow decay of end effects in layered structures with an imperfect interface. J. Eng. Math. **45**, 155–168 (2003)
[28] Bolotin, V.V.: Dynamic edge effect in the elastic vibrations of plates. Inzhenernyi Sbornik Eng. J. **31**, 3–14 (1961)
[29] Lee, P.C.Y., Chang, N.: Harmonic waves in elastic sandwich plates. J. Elast. **9**(1), 51–69 (1979)
[30] Timoshenko, S., Woinowsky-Krieger, S.: Theory of plates and shells, vol. 2. McGraw-Hill, New York (1959)
[31] Prikazchikova, L.: Decay conditions for antiplane shear of a high-contrast multi-layered semi-infinite elastic strip. Symmetry **14**(8), 1697 (2022)
[32] Kaplunov, J., Erbaş, B., Ege, N.: Asymptotic derivation of 2D dynamic equations of motion for transversely inhomogeneous elastic plates. Int. J. Eng. Sci. **178**, 103723 (2022)
[33] Kaplunov, J., Khajiyeva, L.A., Martyniuk, M., Sergaliyev, A.S.: On the dynamics of drilling. Int. J. Eng. Sci. **146**, 103184 (2020)
[34] Goldenweizer, A.L., Lidsky, V.B., Tovstik, P.E.: Free vibrations of thin elastic shells. Nauka, Moscow (1979)

Ludmila Prikazchikova, Julius Kaplunov and Danila Prikazchikov
School of Computer Science and Mathematics
Keele University
Keele ST5 5BG
UK
e-mail: l.prikazchikova@keele.ac.uk

Julius Kaplunov
e-mail: j.kaplunov@keele.ac.uk

Danila Prikazchikov
e-mail: d.prikazchikov@keele.ac.uk

Ameya Rege
Institute of Materials Research
German Aerospace Center (DLR)
Linder Höhe
51147 Cologne
Germany

Ameya Rege
Department of Mechanics of Solids
Surfaces & Systems
University of Twente
P.O. Box 217 AE Enschede
Netherlands
e-mail: ameya.rege@utwente.nl

(Received: May 31, 2024; revised: May 31, 2024; accepted: October 2, 2024)